Ripples in the Ice: Employing ogives to deduce glacier behavior

Tyler James Kane

Department of Geology | University of Colorado at Boulder

Defended November 6, 2013

Thesis Advisor:

Dr. Robert S. Anderson | Department of Geology

Committee Members:

Dr. Charles Stern | Department of Geology
Dr. William (Tad) Pfeffer | Department of Civil, Environmental, and Architectural Engineering
Dr. Robert S. Anderson | Department of Geology

Abstract

Arcuate glacier structures known as ogives are common to valley glaciers flowing below large icefalls and form annually. Long sequences comprising tens of ogives are often preserved on glacier surfaces. We explore their utility as unique sources of information about glacier behavior. Our investigation concentrates on two main objectives: (1) to assess any correlation between an ogive train and a climate time series, and (2) to evaluate what an ogive-derived velocity profile can reveal about the distribution of ice thickness beneath an ogive field. Using ArcGIS software, we analyze high-resolution satellite imagery of the Gates Glacier ogive sequence in southeastern Alaska to document ogive wavelengths, and to produce down-glacier surface velocity and strain profiles. A comparison of ogive wavelengths with the recent climate history from local weather stations suggests a complex relationship between annual temperature, meltwater inputs, basal sliding, and ogive formation. Finally, we employ surface velocity derived from ogive positions on a sequence of images, and a centerline slope profile (acquired from a digital elevation raster), to invert Glen's flow law for an estimate of ice thickness. The calculated ice thickness is then translated to a centerline bed profile and ultimately used to construct a three dimensional view of the Gates Glacier valley geometry.

Introduction

The surficial glacier features known as ogives appear as regularly alternating light and dark bands on a glacier surface, and the phenomenon of their formation is exclusive to locations immediately downglacier of icefalls or avalanche fans. Agassiz first applied the term "ogive" because of the resemblance of the curved layers to the pointed arches in cathedral architecture (in Leighton, 1951). Once formed, these features are parabolic bands (in map view) that span the lateral width of a glacier downstream of icefalls, with the crest of each curve pointing downglacier (Fig. 1).

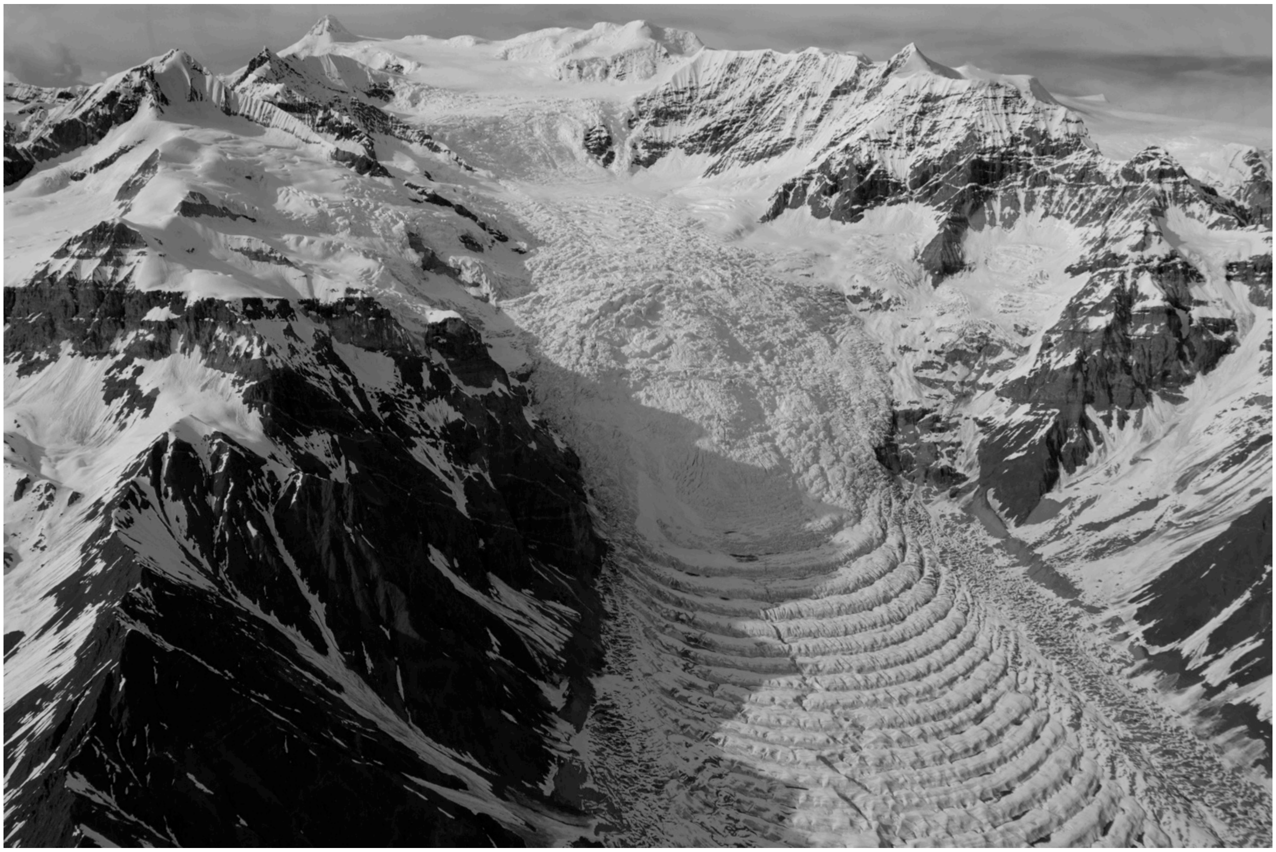

Figure 1. Oblique photo of Gates icefall and ogive train. Photo by Bob Anderson, 2013.

The graceful crescent shapes of ogives have captivated glaciologists since the mid 19th century (Agassiz, 1840; Forbes, 1859). Modern technology has allowed us to further appreciate these features with satellite imagery. While many have argued about the processes responsible for ogive formation, it seems that very few have employed ogives as tools that can provide unique information regarding glacier behavior. The aim of this paper is to investigate the hitherto underexplored role of ogives as valuable assets to further glacier research.

Using high-resolution satellite imagery in conjunction with GIS software, we can characterize the ogive sequence of the Gates glacier of southeastern Alaska, recording ogive wavelengths and planview shapes. The purpose of this study is twofold: one aspect is an analysis of the capabilities of GIS software to automatically discriminate individual ogives, and to compute statistics on the series of ogive lengths on the glacier as a whole. We can then investigate the relationship between the resulting ogive wavelength time series with the history of climate from nearby meteorological station records. Much like rings in a tree, these annually-forming ogives vary in length, presumably reflecting the history of temperature and precipitation from year to year. Second, the ogives can provide us with a surface velocity profile across each glacier. As surface velocity is governed by the thickness of the ice, the surface slope (which we can document from a DEM), and the ice viscosity, the surface velocity field may allow us to deduce ice thickness which is otherwise very difficult and expensive to obtain.

Terminology and field descriptions of ogives

Ogives were originally introduced to the literature in the mid-19th century (Agassiz, 1840; Forbes, 1859), and further investigation spurred much controversy regarding their elusive formation processes. Conflicting observations of ogives complicate a general description, as it seems that each glacier produces bands with slightly different characteristics.

These discrepancies have led to confusion of terminology in the literature, with the interchangeable use of "Forbes bands" (Forbes, 1859), "Alaskan bands" (Fisher, 1947), "ogives" (Leighton, 1951), and "wave ogives" (Fisher, 1962). However, "ogive" has most precedence and utility in describing the large annually forming bands because it has congruent meaning in English, French, and German. A useful distinction made by Goodsell et al. (2002) defines "band ogive" as one pair of light and dark bands. In this definition it is important to note that each larger light region is made up of many narrow structural bands that are *dominantly* composed of light-colored opaque ice, and each larger dark region is comprised *dominantly* of narrow dark-colored ice bands. It is the density of these narrow light or dark bands per unit distance downglacier that defines band ogives (Waddington, 1986). The term "wave ogive" refers to topographic undulations often found near the base an icefall. The amplitude of typical wave ogives, as reported by Waddington (1986), is ~10 m immediately below an icefall, which declines downglacier.

The ogives of the Bas Glacier d'Arolla, as described by Goodsell et al. (2002), first exhibit color differentiation of band ogives at the foot of the icefall, in accordance with the undulating nature of the wave ogives that are developed there. The light-colored bands appear white or light blue and coincide with the upglacier slopes of the wave ogive pressure ridges, while the dark-colored bands appear on the downglacier slopes or in troughs as a darker blue or even brown (Goodsell et al., 2002; Leighton, 1951). The color difference initially becomes more enhanced as the relief of wave ogives declines downglacier. Ogives often become difficult to distinguish or even die out toward the glacier toe. Also noted is the presence of thin zones of dark, highly foliated ice within predominantly light bands, as well as zones of light ice within larger dark bands. Structurally, the dark bands are characterized by a high concentration of surface debris covering highly foliated, "coarse crystalline bubble-poor blue ice" (Goodsell et al., 2002). Conversely, the light bands of ogives are comprised of white, bubble-rich ice, and do not seem to trap surface debris as readily as the dark bands (Leighton, 1951; Clark and Heath, 1955, in King and Lewis, 1961).

Study Area

To understand how ogive sequences can be applied to unveil glacier behavior, it is important that the ogives in question are relatively undisturbed by factors that complicate the ice velocity field, such as uneven valley geometry, sharp turns in flow direction, or secondary ice inputs. Although it is not the only glacier to exhibit well-developed ogives in the region, the Gates Glacier, a major tributary to the Kennecott glacier, is ideal for this study because of its straight geometry, lack of secondary tributaries, and its even valley wall spacing.

The Gates Glacier serves as a tributary to the larger Kennicott Glacier located in the Wrangell Range of southeastern Alaska (Fig. 2).

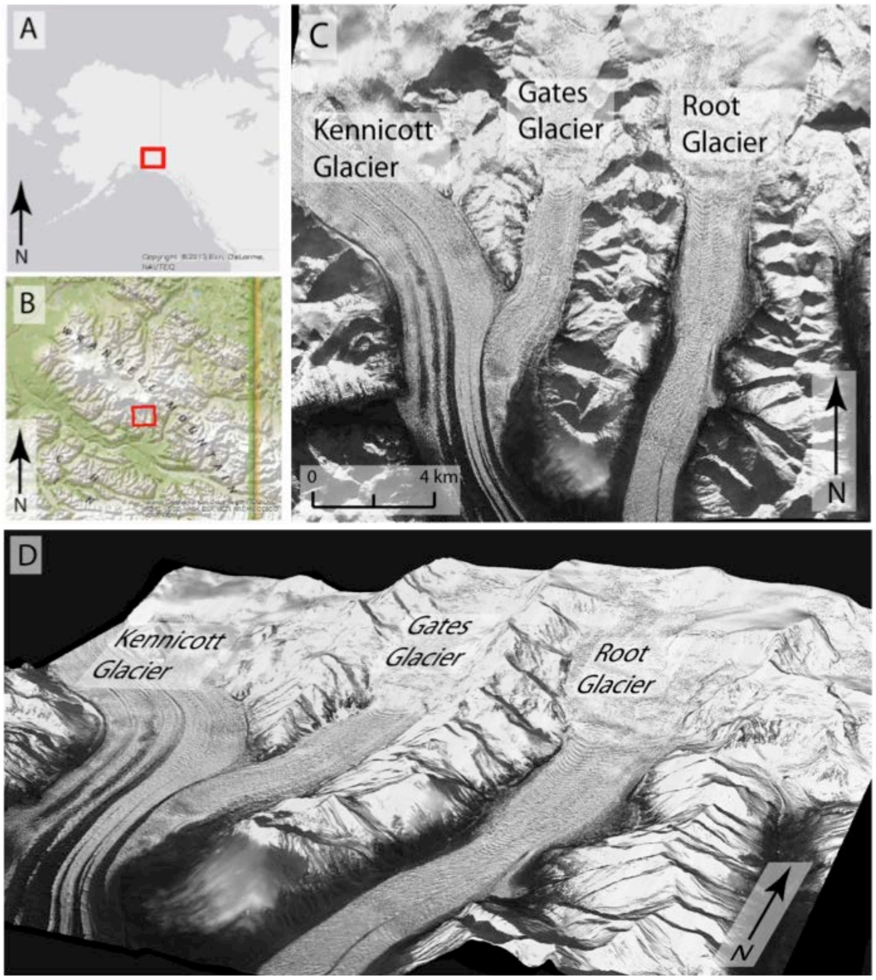

Figure 2. Study Area. (A) Location of Wrangell Mountain Range in southeastern Alaska. (B) Reference map of Wrangell Mountain Range showing topography, indicating the extent of satellite imagery. (C) World View 1 image including the Gates and Root Glaciers, and the Kennicott Glacier terminus. (D) Oblique view of the study area image draped over a 1/3 arcsecond DEM of 10 m spatial resolution (National Elevation Dataset).

The Gates Glacier transports ice southward from the central Wrangell peaks through a two-tiered icefall (Fig. 1) and down along a 5 km valley before merging with the Kennicott Glacier. The total length of the icefall feeding the glacier is over 6 km, initially climbing 700 m along the first 2 km north of its base. Then the slope levels off for the next 2.5 km and only gains another 250 m in elevation. The second tier of the icefall begins 4.5 km from the base of the icefall and climbs another 750 m before reaching the top of the icefall, accumulating a total elevation gain of nearly 1700 m. The cross-glacier width of the Gates Glacier valley is ~1700 m, and the total area covered by both the icefall and glacier below it is ~23 km^2.

The imagery of the Gates Glacier was taken by the World View 1 satellite on October 6, 2009, at the beginning of the winter season. The 0.5 meter spatial resolution lends an exceptionally detailed view of the Gates Glacier ogives (Fig. 3). A layer of snow covering the

Figure 3. Detailed view of the Gates Glacier. (A) Upper portion of the Gates Glacier, showing entire ogive train. (B) Ogive formation at icefall base. (C) Well developed wave ogives and supraglacial streams. (D) Ogives become difficult to distinguish downglacier, wave ogives disappear, and band ogives become pronounced.

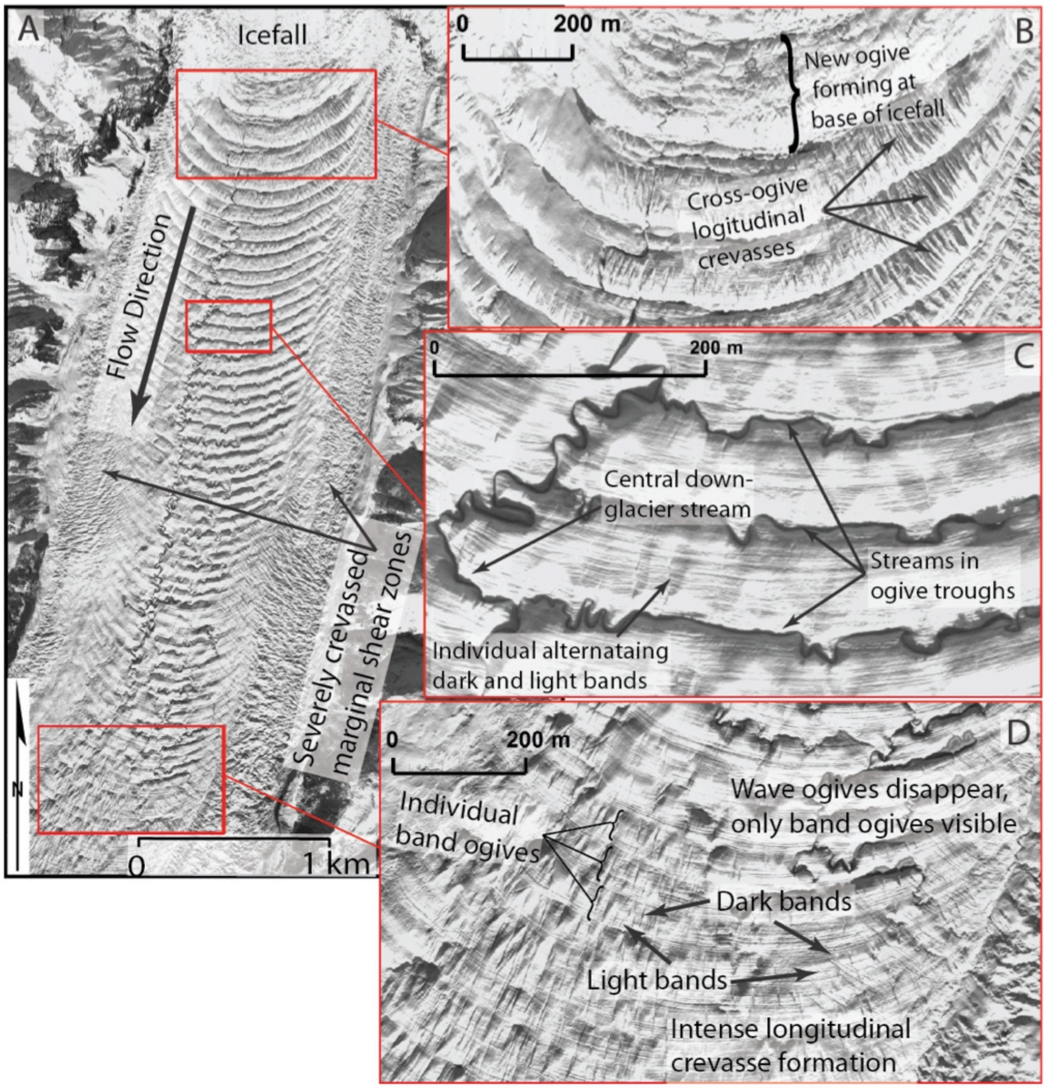

glacier and the surrounding region at the time of the photograph makes band ogives difficult to identify, but the sun's illumination angle accentuates the well-preserved wave ogives. The ogives in the World View imagery appear as broad, rounded, light-colored ridges, bounded by narrow troughs. A major waterway incised generally parallel to ice flow, transports supraglacial meltwater downglacier, which is further carried through the ogive troughs to the glacier margins. The networks of streams running parallel to the ogives help to discriminate one ogive from another. Discrete crevasse formation is apparent on many of the ogive ridges, trending orthogonal to the arcuate shape of the ogives. Nearly 50 ogives can be identified along the glacier length, although they become increasingly difficult to differentiate as deformation and crevasse formation modifies the downglacier ice (Fig. 3D). The young ogives near the base of the icefall have wavelengths of 100-250 m, and extend laterally to severely crevassed zones along the glacier margins. These marginal shear zones are between 150 m and 450 m in width, where significant deformation makes ogive differentiation impossible. Compressional stress acting parallel to flow generates strain that reduces ogive wavelengths to less than 100 m after Ogive 5, reaching a minimum of ~60 m before the ogives become indistinguishable nearly 4 km downglacier from the icefall.

Ogive Formation

Periodicity of Formation

Although it is generally accepted that the frequency of ogive formation is one ogive per year, it is essential that we solidify that assumption before continuing on to further investigations. With the wide availability of detailed repeat satellite imagery, simple feature tracking along a glacier surface can be done with ease. To demonstrate this, two images of a glacier surface can be compared to see how stream channels move downglacier (Fig 4). Figure 4B shows a portion of the central stream from the upper Gates Glacier from Google Earth imagery taken on September 11, 2010. This stream was traced in red and imported into ArcGIS to be compared the World View 1 image taken on October 6, 2009 (Fig. 4C). The same section of stream from 2009 is digitized in blue. Rough measurements of displacement on distinct stream elbows indicate surface velocities between 60 and 100 m/yr, reasonable estimates for the Gates Glacier (Fig. 4C). Although the stream geometry changed slightly over the 11-month timespan, the total stream displacement is almost exactly one ogive length. Therefore they are clearly annual features, and we can now assign a year of formation to each ogive. The superimposed 2009 and 2010 streams displayed Figure 4D provides an interesting view of the slight variations in stream geometry. Questions arise regarding the interaction between crevasses, longitudinal compression, and the inherent meandering nature of streams. Whatever implications this has for supraglacial stream evolution may be an intriguing topic of future study.

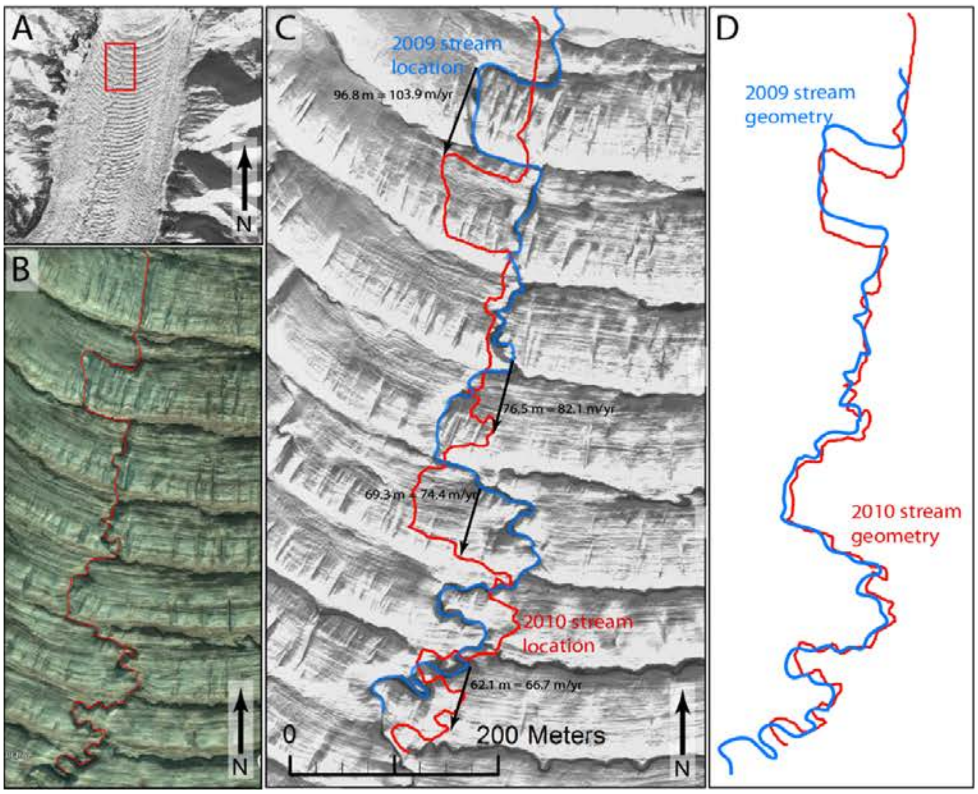

Figure 4. Ogive periodicity. (A) Reference map showing the location of a portion of the central Gates Glacier stream. (B) Google Earth image from 2010. The section of stream has been traced in red. (C) The same section of stream in the World View 1 image (from 2009) traced in blue, including the 2010 stream location. Rough velocities were calculated from stream displacement. (D) The traced 2009 (blue) and 2010 (red) stream geometries superimposed on one another.

Proposed ogive formation mechanisms

Much of the dispute among glaciologists has arisen in regard to the formation of band ogives. Early analyses argued that band ogives were a result of the original sedimentary stratification of the firn as it is carried through an icefall (Hess, 1904, in Goodsell et al., 2002; Agassiz, 1840). The dark bands are a product of dust and debris accumulation on summer ice passing through an icefall, while winter snowpack covering the region would prevent the sullying of winter ice, producing white banding. This was supported by pollen studies by Vareschi (in Godwin, 1949). Vareschi found that the white bands of band ogives contained only winter ice while the dark bands contained spring, summer, and autumn pollen. However, this theory has been widely discounted, as any sedimentary layers would be destroyed while passing through the icefall tumult. Some call upon the accumulation of surficial dust and debris within transverse crevasses that open during the extensional flow in an icefall. Upon reaching the icefall base, debris-filled crevasses compress to form dark bands and the intervening ice blocks compact to form white bands (in Leighton, 1951: Tyndall, 1876; 1896; Scherzer, 1907; Washburn, 1935; Streiff-Becker, 1943). However, the application of this hypothesis is compromised by the lack of glacier-wide crevasses in every ogive-producing icefall (Leighton, 1951).

Others have suggested that the acceleration of ice through an icefall stretches and thins the ice; summer ice on the steep icefall slope collects more eolian dust and ablates more readily than ice passing through during the winter. The large negative velocity gradient between the icefall and the gentler slope of the glacier surface compresses dirty summer ice to form a dark trough, while winter ice forms a light ogive ridge (Nye, 1958, 1959; Miller, 1949; King and Lewis, 1961; Fisher, 1962). This relatively simple hypothesis is well based in the principles of mass conservation, but appears to fail to explain some ogive field observations. For example, the dark regions of band ogives tend to be concentrated on the downglacier slopes of waves, and not in the center of the troughs. Moreover, some debris found within ogives is too coarse to have been transported by wind, and much of it appears to have been subjected to sub-glacial modification (Goodsell et al., 2002; Leighton, 1951).

More recent investigations have acknowledged the importance of the spatial concurrence of band ogives and wave ogives, which indicates a structural mechanism for ogive formation. In his mathematical analysis of wave ogive formation, Waddington (1986) builds upon Nye's (1958) ablation-plastic stretching mechanism to conclude that gradients in ice velocity, mass balance, or channel width can create waves, but “only large and localized gradients traversed by the ice in 6 months or less can generate waves sufficiently coherent to form large wave ogives.” Goodsell et al. (2002) rely on these well-understood physical principles along with rigorous field observations and ground-penetrating radar data to develop a convincing structural mechanism for ogive genesis.

In this model, ice passing through an icefall undergoes extensional flow, which induces lateral as well as longitudinal crevasse formation. Sedimentary stratification is also observed within the icefall. While passing through the base of the icefall, the negative velocity gradient produces strong compressional stress. This not only results in the deformation of sedimentary strata and the closure/folding of crevasses, but also the formation of highly foliated shear zones (Fig. 5). Following ideas proposed by Posamentier (1978), Goodsell et al. (2002) call upon small-scale reverse faulting to accommodate compressive flow at the icefall base. Seasonal mass balance variations initiate slip as compressional stress breaches a brittle failure threshold within the ice with annual periodicity. The annual slip is expressed on the glacier surface as a train of fault-related folds: the alternating troughs and ridges of wave ogives. The amplitude of these folds attenuates downglacier with ablation, leaving behind alternating bands of high foliation and low foliation. Contrary to Posamentier’s theory, large fault surfaces are not exhibited at the ice surface. Goodsell et al. attribute this absence to the distribution of annual slip to many smaller faults rather than along a single large fault surface. A single group of these small fault surfaces together form a dark-colored, foliation-rich shear zone: a dark band. The foliation is detected by GPR as reflection-rich bands dipping upglacier. Most importantly, Goodsell et al. assert that the color difference of band ogives is not due to debris content, but instead can be explained by the varying intensity of foliation.

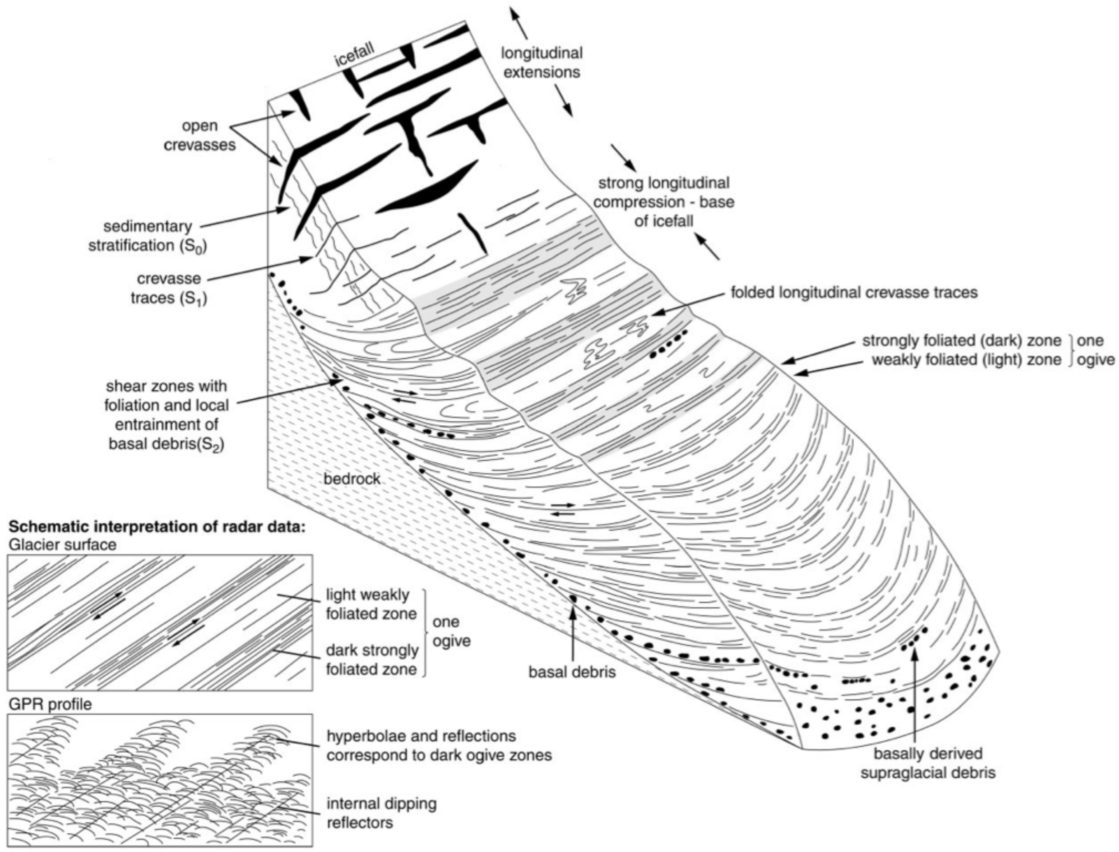

Figure 5. Ogive production due to annual reverse faulting and associated drag folding (image from Goodsell et al, 2002).

While there remains some dispute between Nye's original ablation-plastic stretching mechanism and the reverse faulting mechanism, both theories require annual variations in mass balance to drive changes in the velocity gradient across the icefall base. The first segment of this investigation will attempt to isolate these seasonal mass balance variations by documenting ogive wavelengths on the Gates Glacier.

Part I: Ogives as Tree Rings

The three possible ogive-forming factors established by Waddington (1986) are gradients in velocity, valley geometry, and mass balance. We can assume that valley geometry remained constant during the formation of the visible Gates ogive sequence, yet we observe variations in ogive wavelength within the sequence. These fluctuations are slight, but erratic, and are most likely not attributable simply to compressive strain or any other post-formation modification. Because ice velocity relies on bed slope and ice thickness, it is 2logical to call upon annual changes in mass balance to produce slightly different ogives from year to year.

Before comparing the Gates Glacier ogive sequence to local weather data, it is important to eliminate as much human error in the wavelength measurement as possible. Although the streams running along the troughs make the ogives distinct from one another when viewed from a great distance, their meandering nature gives rise to measurement uncertainty when viewed from a closer vantage point. Moreover, increased compressional deformation further downglacier is problematic for discriminating one ogive from another. Fortunately, the sun angle generates regular shadows on the upglacier side of each wave ogive, which can be recognized and analyzed by ArcGIS. Another major advantage of processing the imagery in ArcGIS is our ability to automate our methods, so that analyzing an entire ogive sequence can take seconds, rather than hours, and the process can be easily translated from one glacier image to another.

Methods for measuring ogive wavelength in ArcGIS

The World View 1 raster imagery consists of grayscale pixel color values ranging from 0 (black) to 255 (white). Much like the "Interpolate Line" tool available in ArcMap, which interprets pixel values along a line, we call upon the software to compute statistics on color pixel frequency along a wider swath. This is done in an effort to smooth out any noise generated by imperfections or roughness on the glacier surface. We start by creating a polyline shapefile in ArcMap of the downglacier profile from the base of the icefall to the last distinguishable ogive in the sequence. Careful placement of the profile is very important. The Gates Glacier profile is drawn generally perpendicular to each ogive curve near the center of the glacier, while avoiding the main downglacier supraglacial stream.

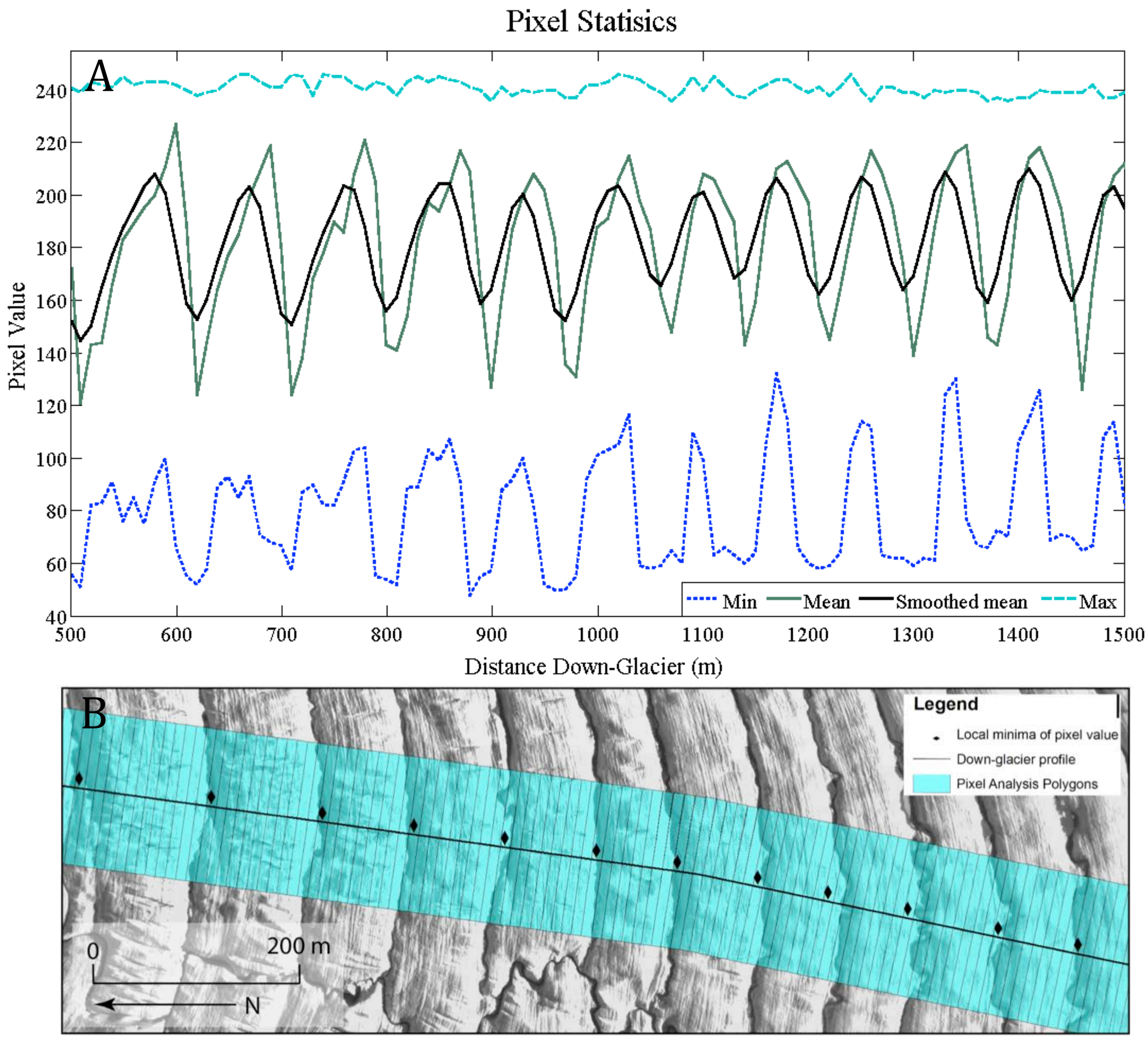

Figure 6. Ogive trough isolation. (A) Pixel brightness statistics plotted against distance downglacier. Ogive distinction is defined by the local minima of the smoothed mean. (B) Gates Glacier ogives in ArcGIS with downglacier profile (black). Analysis polygons (blue) and point locations of local minima (black diamonds) are direct outputs of the python script. Note that the portion of the downglacier profile represented in (A) corresponds to the glacier region shown in (B).

Once the profile is drawn, the software is prompted to create a train of rectangular polygons (with dimensions as indicated by the user) centered on the profile. The chosen length (parallel to the profile) should be significantly less than the average ogive wavelength, and the chosen width (orthogonal to the profile) should be such that ogive curvature cannot be easily recognized within the bounds of each box. For the Gates Glacier, we define these rectangles to be 10 m in length, and 150 m in width (Figure 6B). Next, the program computes the maximum, minimum, and mean values of all pixels contained within each rectangle, and reports these data with respect to the distance of the center point of each box from the icefall (Figure 6A). We then apply a smoothing algorithm to the mean pixel values, and isolate the local minima. These minima correspond to regions along the profile with the highest concentrations of dark pixels, effectively isolating the shadowed ogive troughs. Finally, we input the locations of these isolated minima back into ArcMap as a shapefile consisting of a list of geographic points, displayed as small black diamonds in Figure 6B. Note that the predicted locations of ogive troughs are slightly upglacier of where they actually appear. This is a product of the smoothing algorithm, but this effect should not mar the validity of the overall ogive sequence, as the downglacier shift is applied evenly throughout the whole profile (Figure 6). While this technique is effective, we further reduce error in the wavelength measurements by drawing not just one but three parallel downglacier profiles (each separated by ~25 m), and computing the overall average ogive locations and ogive wavelengths. In effect, this serves to lower the noise associated with random variations in color of the forms, much as stacking of seismic profiles lowers the noise.

The final step in preparation for this analysis is to remove any influence from compressional strain from the observed ogive record. If the bed slope beneath the ablation zone of a glacier remains relatively constant, the surface ice velocity should decrease with distance downglacier as the ice thins toward the terminus. Therefore, a given parcel of surface ice would have a slightly lower velocity than the parcel immediately upglacier. The resulting compressional strain acts parallel to flow, and is reflected in the broad trend of ogive wavelength shortening that we observe in the Gates Glacier ogive sequence. To attain an undistorted wavelength record, we must isolate and reverse the effects of strain from each ogive. We can approximate total strain, Ɛ, experienced by an individual ogive at *x* meters from the icefall with the following relationship:

$$\int_0^T \frac{\partial u}{\partial x} dt \cong \varepsilon \;, \tag{1.1}$$

where *u* is the mean velocity (in m/yr), *t* is time (in years), and *T* is the number of years since the formation of the ogive. Because some of the mean velocity is due to basal sliding, we can approximate by using measured surface velocities (Cuffey and Paterson, 2010). Surface velocities at various distances downglacier were calculated by tracking ogives in repeat imagery available on Google Earth, which were then plotted and fit to a curve (Fig. 7).

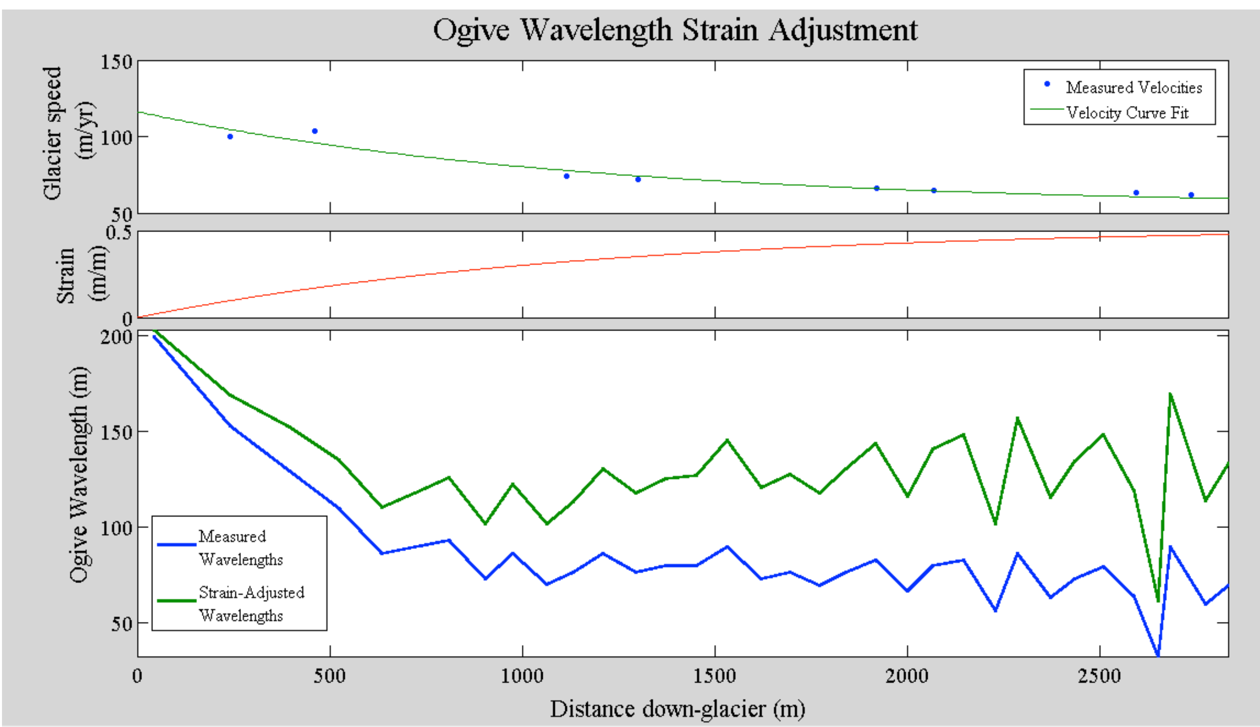

Figure 7. Reversal of the strain effects on ogive wavelengths. (Top) Measured surface velocities and fitted velocity curve, (Middle) accumulated strain, and (Bottom) measured and strain adjusted ogive wavelengths, all plotted with respect to distance downglacier.

In Matlab, a hypothetical ogive 100 m in wavelength was created and placed at the base of the icefall. Then stepping forward through time at 0.01 year intervals for 50 years, the locations of the top and bottom boundaries of the ogive were extracted from the velocity curve. 1-D compressional strain is defined as follows:

$$\varepsilon = \frac{L_o - L}{L_o} \quad , \tag{1.2}$$

where L is the measured ogive wavelength of an ogive and L_o is the predicted original length of the ogive before any compressional strain was applied. By applying this definition at each time interval, we can define $\varepsilon(x)$ as the total strain modifying the ogives as a function of x, the distance (in meters) down glacier (Fig. 7). Therefore, we are able to estimate each ogive's undeformed (or original) wavelength by rearranging (1.2):

$$L_o = \frac{L}{1 - \varepsilon(x)} \quad . \tag{1.3}$$

In Figure 8 we display the original ogive sequence plotted with annual snowfall accumulation and positive degree-days (PDD) between 1976 and 2008. These are records derived from the McCarthy airport weather station, located 20 km south of the Gates Glacier.

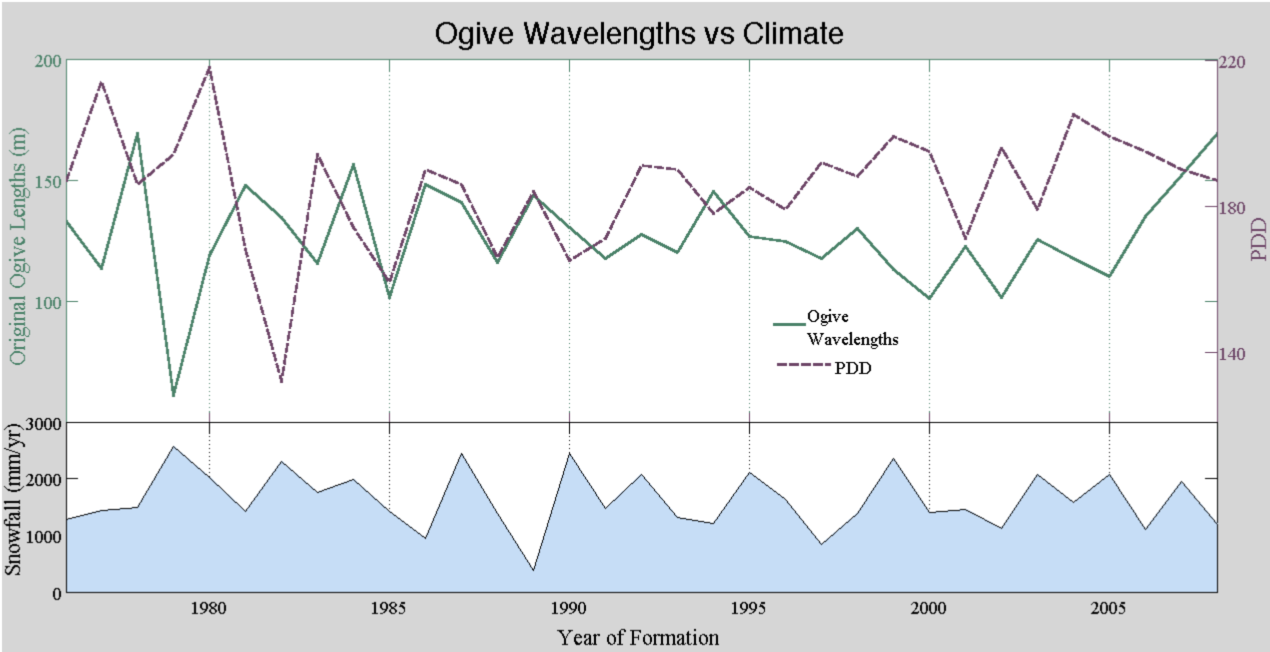

Figure 8. Comparison of ogive sequence to climate records. Ogive wavelengths (adjusted for strain) are plotted on the left vertical axis, positive degree days on the right vertical axis, and annual snowfall (in mm/yr) is plotted below, all with respect to year of ogive formation.

Discussion of Ogives as Tree Rings

The Gates Glacier ogive sequence preserves well-developed ogives between the years 1976-2008. Wavelengths (adjusted for longitudinal strain) fall between $61.3\ m$ and $202.9\ m$ with a mean wavelength of $129.3\ m$, the range of PDD is between 132 and 218 $days/yr$, with an average value of 218 $days/yr$, and snow accumulation ranges from 371 and 2561 mm/yr, with a mean of 1623 mm/yr. However, there appears to be no direct year-to-year correlation between ogive wavelength and either the PDD or snowfall records. When comparing ogive wavelength and snow accumulation, we find these records are not consistently in phase or out of phase. The same seems true for ogive wavelengths and PDD, although they are briefly well aligned between 1984-1990. When the climate time series are normalized and plotted against the normalized ogive wavelengths in Figure 9, it becomes even more clear from the relatively even spread of climate data that there is very little annual correlation between the sequence of ogive wavelengths and the available PDD and snow accumulation records.

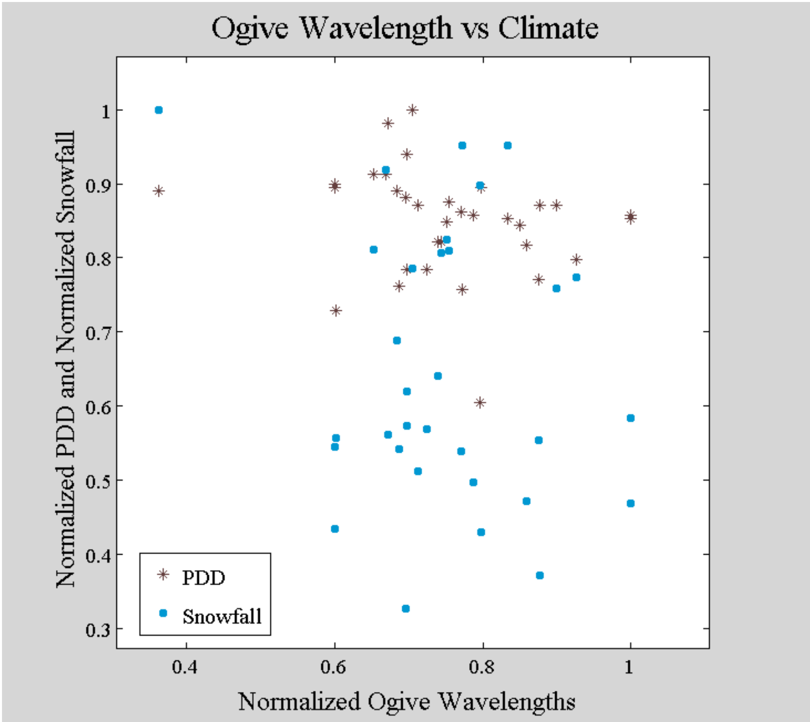

Figure 9. Comparison of normalized ogive wavelengths with normalized PDD and snowfall records. The broad spread of data indicates little year-to-year correlation.

However, when viewed over broad multiyear time scales, Figure 8 may capture some more subtle relationships between PDD and ogive wavelengths. For example, the amplitude of oscillation between longer and shorter wavelengths seems to scale with that of warmer and cooler years. From 1998 to 2005, ogive wavelengths regularly oscillate between $130\ m$ and $100\ m$, while the number of positive degree-days per year during this timespan alternates between 195 and 170. We see much greater amplitudes in both records during the years 1976-1983; wavelength varies from nearly $170\ m$ to $61\ m$, while PDD ranges from $214\ days/yr$ to $132\ days/yr$.

Figure 10. Smoothed climate to wavelength comparison. Ogive wavelengths and the PDD record from Fig. 8 are smoothed and plotted together on the same vertical axis, against year of ogive formation on the horizontal axis.

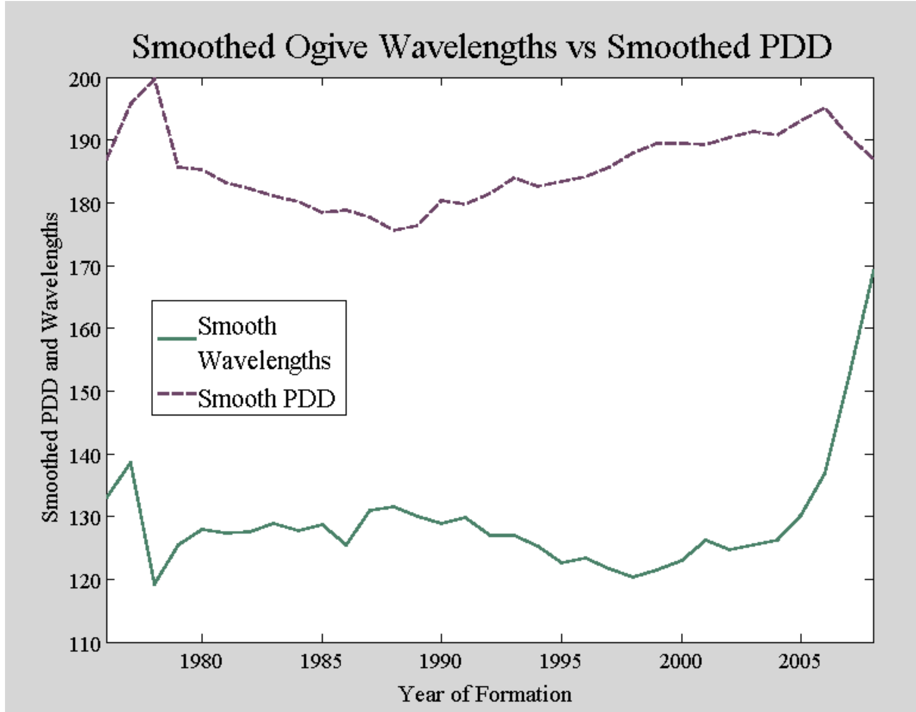

Furthermore, we find a broad negative correlation between ogive wavelength and PDD, but only over the 30-year timescale preserved by the entire ogive sequence. While difficult to detect in Figure 8, it is more apparent in Figure 10, in which year-to-year noise is smoothed out of both records. Here we see PDD reduction from values of 190 to 176 between 1978 and 1988, followed by a steady rise to a local maximum of 195 in 2006. The record of ogive wavelengths appears to form a mirror image of PDD. During 1978-1988 ogive wavelengths increase from 119 m to 131 m, and then steadily decrease to 120 m in 1998. The alignment of the wavelength local maximum and the PDD local minimum in 1988 further supports a decadal-scale negative correlation between the two records, which ultimately suggests that longer ogives form in cooler years.

However, the dependence of ogive wavelength on PDD is vague, which indicates more complex factors controlling ogive formation than simply the influence of temperature and snowfall. The link between cold years and longer ogive wavelengths relates temperature and surface ice velocity, which can be broken into components of basal sliding and internal deformation. One product of higher air temperature is increased surface melting, which would serve to deliver more liquid water to the glacier bed. Hydrological investigations of the Greenland ice-sheet indicate a correlation between the timing and intensity of surface melting and surface ice velocity (Zwally et al., 2002; Bartholomew et al., 2010). The work of Harper et al. (2007) on the Bench Glacier revealed two distinct phases of dramatically increased sliding during the transition from winter to summer. And on the Kennicott Glacier itself, there is clear speed-up of the glacier associated with the state of the hydrologic system, where the "rise in stored englacial water increases the pressure head at the bed, which reduces the effective pressure at the bed and promotes basal motion" (Batholomaus et al., 2007; 2011).

We are now led to question the influence of meltwater to the sliding velocity of an icefall. While the highly crevassed nature of an icefall would enable more meltwater to percolate to the underlying bed, it may be that the high permeability also inhibits sufficient pressure to build beneath an icefall. Under this assumption, it follows that the introduction of meltwater to a glacier more effectively increases the mean velocity of ice below an icefall than it does for the velocity of the icefall itself. Therefore, the velocity gradient across the base of an icefall will be *reduced* during a warm year in which increased melting leads to higher velocity below an icefall. Conversely, decreased amounts of meltwater delivered to the bed during a cold year would result in lower velocity below the icefall, and ultimately a *greater* velocity gradient across the icefall base. Cold years in which the velocity gradient is large would presumably increase the distribution of reverse fault slip to a larger number of fault planes. This would result in a longer wave ogive wavelength, as well as a band ogive with a broader section of dark, foliated ice.

It remains very difficult to separate sliding velocity from internal deformation, and constraining the contributing variables to sliding velocity is equally enigmatic. Potential issues with these interpretations arise when dealing with sliding velocities, and in particular, when comparing behavior of ice-sheets, valley glaciers, and icefalls. While, the subglacial hydrological system below an ice sheet may highly contrast that of a valley glacier, it is clear that the state of the hydrologic system within and beneath glacier ice is a primary factor in basal sliding (Zwally et al., 2002; Bartholomew et al., 2010; Batholomaus et al., 2007; 2011, Harper et al., 2007). Yet more problematic are the physics of chaotic icefall behavior, which remains very poorly understood, and poorly documented.

The first step in any future work on this project would begin with a re-examination of the climate data used to compare with ogive sequences. The McCarthy Airport records of average daily temperature do not include nighttime temperature. Although this skews the temperature sums toward higher annual values, the year-to-year temperature fluctuations relative to one another should not be dramatically affected. These records are adequate for an initial investigation of this problem, but more robust data (e.g. NCEP/NCAR Reanalysis) would be needed for a deeper exploration of the correlations.

An interesting potential study could attempt to document carefully the genesis of a single ogive from icefall to glacier surface. An important component of this project is to increase our understanding of how icefall and glacier surface velocities vary when exposed to the same climatic conditions. GPS stations placed high on the glacier surface near the icefall would be needed to calculate glacier surface velocities. However, GPS devices would be difficult to place and retrieve (and may not survive) on an icefall, so establishing year-round icefall velocities would involve training a camera upon an ogive-producing icefall for 2-3 years. Combining these observations with hydrologic and climate data could potentially reveal much about icefall behavior, as well as the velocity gradient involved in the generation of an ogive.

Part II: Estimations of Ice Thickness

Glen's flow law dictates that variations in glacier behavior are extremely sensitive to subtle changes in ice thickness and surface slope. While surface slope is relatively easy to obtain from digital elevation models, direct measurements of ice thickness remain tedious and expensive to acquire. Developing an understanding of the distribution of ice thickness throughout a glacier may quell a broad range of contentious glaciological, hydrological, and climate-related issues (Farinoti et al., 2009). For example, numerical models representing past and present glacier extents often require ice thickness values as primary inputs (Hubbard et al., 1998; 2009), and the mass-balance solutions to these models are critical to investigations of the impacts of climate change. The total ice volume within a glaciated valley or ice-sheet scales with ice thickness, and defines the amount of stored water, which yields important implications for global sea level rise (Pfeffer et al., 2008), and for local watershed storage. Furthermore, knowledge of ice thicknesses would aid in attempts to isolate the contribution of surface ice velocity due to basal sliding from that of internal deformation. In turn, distinguishing environmental factors that influence basal sliding could enhance our knowledge of glacier bed erosion rates, as well as future rates of calving and ablation.

Historical estimates and modern measurements

Historically, ice thickness has been roughly estimated by approximating glacier ice as an ideal plastic material where the bed stress, τ^*, and the yield shear stress, τ_o, satisfy the following:

$$\tau_o = \tau^* = \rho g H sin(\alpha) \ , \tag{2.1}$$

where ρ is the density of ice, g is the acceleration due to gravity, and α is the angle of ice surface slope. If the slab of ice is in "plastic equilibrium," there is a defined thickness for every slope α (Orowan, 1949; Clarke et al., 2012). We can rearrange Equation (2.1) to yield ice thickness, H:

$$H = \frac{\tau_o}{\rho g sin(\alpha)} \quad . \tag{2.2}$$

This calculation assumes an infinite lateral extent, such that wall drag has no effect, and commonly a basal stress of $1\ bar\ (= 10^5\ Pa)$ is used: $\tau_o = 1\ bar$. However, this value is not a physical property for all glacier ice, and wall drag has been found to significantly affect basal shear stress (Nye, 1965). These assumptions considerably limit the utility of (2.2) for estimating ice thickness (Clarke et al., 2012).

Modern methods for acquiring direct measurements of ice thickness include GPR, borehole measurements, and seismic reflection. The presence of liquid water within temperate glacier ice significantly reduces the high resolution of GPR, and borehole measurements are time consuming and laborious. The density contrast between ice and the underlying bedrock is advantageous for compiling a seismic reflection profile, but configuring geophone arrays is labor-intensive, and setting off explosive charges on a glacier surface is not often feasible, especially in a National Park.

To circumnavigate these difficulties, we employ ogive displacements from repeat satellite imagery, along with a DEM-derived surface slope profile to develop an ice thickness approximation. A partial bedrock elevation profile of the Gates Glacier is ultimately produced from a manipulation of Glen's flow law, further modified by Nye's (1965) assessment of the effects of valley geometry on wall shear strain.

Theory behind ice thickness estimation

We begin under the assumptions that the density of ice, ρ_i, is incompressible, and that it flows with a centerline velocity, U_o, at any given height above the bed, z, in accordance with Glen's flow law describing the rheology of ice:

$$\frac{dU_o}{dz} = A\tau^n \ , \tag{2.3}$$

where A is a flow-law parameter, τ is the shear stress within the glacier, n is an experimentally determined rheology parameter. We can expand (2.3) by further defining the shear stress τ as a function of height, z, and α, the angle of the surface slope from horizontal:

$$\tau = \rho_i g(H - z)sin(\alpha). \tag{2.4}$$

Here we define H as the total ice thickness and g is the acceleration due to gravity. Glen's (1952) experiments revealed that the rheology of ice is roughly cubic, so we will designate $n = 3$. Inserting this into the general form of Glen's flow law, we are left with:

$$\frac{dU_o}{dz} = A[\rho_i gsin(\alpha)]^3(H - z)^3 , \tag{2.5}$$

Next, we integrate the shear strain rate $\frac{dU}{dz}$ with respect to z, and evaluate at $H = z$ to obtain the surface speed along the centerline, U_o:

$$U_o = A[\rho_i gsin(\alpha)]^3 \left[\frac{H^4}{4}\right] . \tag{2.6}$$

If we set $A = 6.28 * 10^{-24}\ Pa^{-3}s^{-1}$ (MacGregor et al., 2000), $g = 9.81\ m/s^2$, $\rho_i = 917\ kg/m^3$, then surface velocity becomes a function of surface slope, α, and ice thickness in meters, H.

However, it is important to remember that a glacier surface velocity is the sum of two velocities: the surface velocity attributable to internal deformation, and that associated with basal sliding. Glen's flow law only accounts for internal deformation of a fluid, and we must assume that some fraction of our measured velocities is due to basal sliding. Let this fraction be f_s such that the velocity due to internal deformation alone is given by:

$$u_{def} = (1 - f_s)[U_o(H, \alpha)] . \tag{2.7}$$

Furthermore, the simple application of Glen's flow law embedded in (2.6) assumes infinitely wide valley geometry, and therefore fails to acknowledge the influence of shear strain from the glacier valley walls.

Before implementing the ogive velocity profile into Glen's flow law, it is important that we identify the influence of the glacier valley geometry on the measured velocities themselves. We begin by assuming the geometry of the Gates Glacier valley to have a symmetrical semi-elliptical shape, with a maximum centerline depth H, and cross-valley width of $2W$. Approaching the problem conceptually, imagine a valley whose cross-sectional area is semi-circular, or where $\frac{W}{H} = 1$. Shear strain from the walls of this valley will heavily influence the velocity of glacier ice flowing through it. Conversely, a valley whose cross-valley width is far greater than its maximum depth, in which $\frac{W}{H} \to \infty$, has the shape of an infinitely wide semi-ellipse. In this case, the contribution of shear strain from the valley walls approaches zero at the valley centerline, and therefore the surface ice velocity is left uninhibited; equation (2.6) should be appropriate. The shear stress τ along the centerline for non-circular channels approaches the linear function:

$$\tau = f\rho_i g(H - z)sin(\alpha), \tag{2.8}$$

where f is an adaptation of Nye's (1965) numerically derived shape factor, which calculates the total shear stress including the additional shear stress from wall drag (Cuffey and Paterson, 2010).

W	f
1 (circular valley)	0.5
2	0.709
3	0.799
4	0.849
30 (infinitely wide)	1

Table 1. Shape factor f for calculation of shear stress on the centerline, where W represents the half-width/thickness. Adapted from Cuffy and Patterson, pg 342.

Table 1 reports values of f for a semi-elliptical valley with a given non-dimensional ice thickness, $H = 1$, and a varying non-dimensional half-width, W. Passing from (2.3) to (2.6) demonstrates that surface velocity U is proportional to τ^n, and therefore we can relate the shape factor based upon shear stress f to a correction factor relevant to surface velocity with $f^n = f^3$. The Gates Glacier valley is *not* infinitely wide, and therefore, the shear strain from the valley walls will slow the glacier ice, U, to some fraction of the surface velocity expected in an infinitely wide valley, U_o, such that $f^3 = U/U_o$. The values of f from Table 1 are plotted in Figure 11A as $f^3 = U/U_o$ against $2W/H$, the ratio of the full valley width to depth, and then fit to an asymptotic exponential curve. Because H is held constant, the ratio U/U_o is a function of only W, and we refer to this function as $R(W)$, given by Equation (2.9):

$$R(W) = 0.125 + 0.875\left(1 - e^{\left(\frac{1-W}{W_*}\right)}\right) , \tag{2.9}$$

where the fitting parameter $W_* = 3.65$. As the full width of the Gates Glacier valley, including its shear margins outboard of the identifiable ogives, is sufficiently uniform at ~1700 m, we can set $W = 850\ m$. We can then express R in terms of the valley depth, H, as demonstrated in Equation (2.10):

$$R(H) = 0.125 + 0.875\left[1 - e^{\left(\frac{1-\left(\frac{850\ m}{H}\right)}{3.65}\right)}\right] . \tag{2.10}$$

Next, we limit H to a set of depths between $H_{min} = 200\ m$ and $H_{max} = 850\ m$, and plot $R(H)$ in Figure 11B.

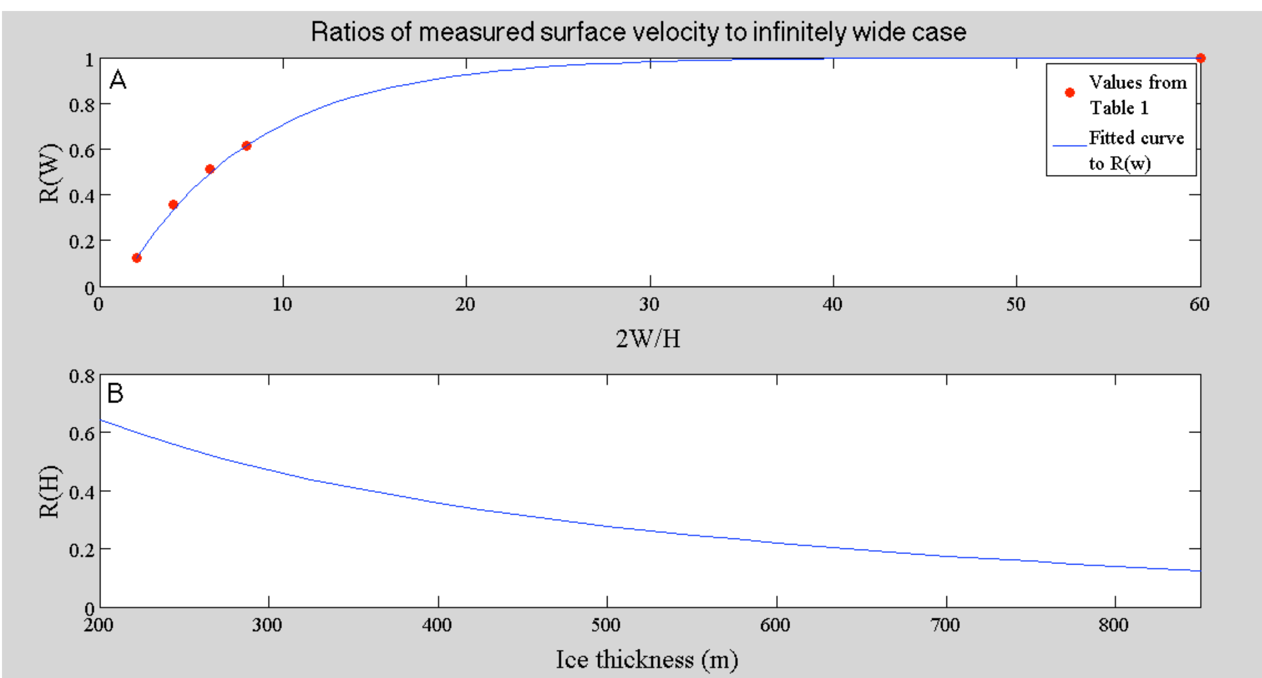

Figure 11. Ratios of measured surface velocity U the velocity of an infinitely wide glacier, U_o. (A) Plot of points from Table 1, fit to the curve $R(W)$. (B) $R(W)$ is converted to $R(H)$ by defining the Gates valley half-width as $W = 850\ m$.

Recall that $R(H)$ represents the ratio U/U_o as a function of H. It follows that for a given H and α, we can arrive at a surface ice velocity U by multiplying $R(H)$ with $[U_o(H,\alpha)](1-f_s)$:

$$U = R(H)[U_o(H,\alpha)](1-f_s) \tag{2.11}$$

Surface slopes can be documented along a down-glacier profile from a DEM and subsequently inserted into Equation (2.6) such that U_o remains only a function of H:

$$U = (1-f_s)R(H)U_o(H) \tag{2.12}$$

Equation (2.12) illustrates that a glacier with a uniform sliding fraction f_s has a unique surface velocity U for every ice thickness, H. Therefore, an array of measured surface velocities can be applied to generate an array of ice thicknesses that vary downglacier.

Results and Discussion

The Gates Glacier velocity profile from Part I is used here. Again, surface velocities were acquired by measuring the displacement of individual ogives in Google Earth, and dividing by the time increment between images. Downglacier surface slopes were calculated and smoothed along the Gates Glacier centerline from a DEM. Throughout the calculations, we assumed three values for f_s: 0.2, 0.5, and 0.8 that ought to bracket the likely sliding contribution. The measured centerline velocity profile and surface slope profile are plotted (Fig. 12A and 12B) above a plot of the downglacier elevation profile with three calculated centerline bed elevation profiles, one for each value of f_s (Fig.12C). Note that Figures 12A, 12B, and 12C are plotted against distance down glacier, and all are lacking the region between 0 and $500\ m$ from the icefall. The slope profile in this region is too chaotic due to the influence of the large wave ogives, and the section was omitted to prevent over-smoothing of the slope profile.

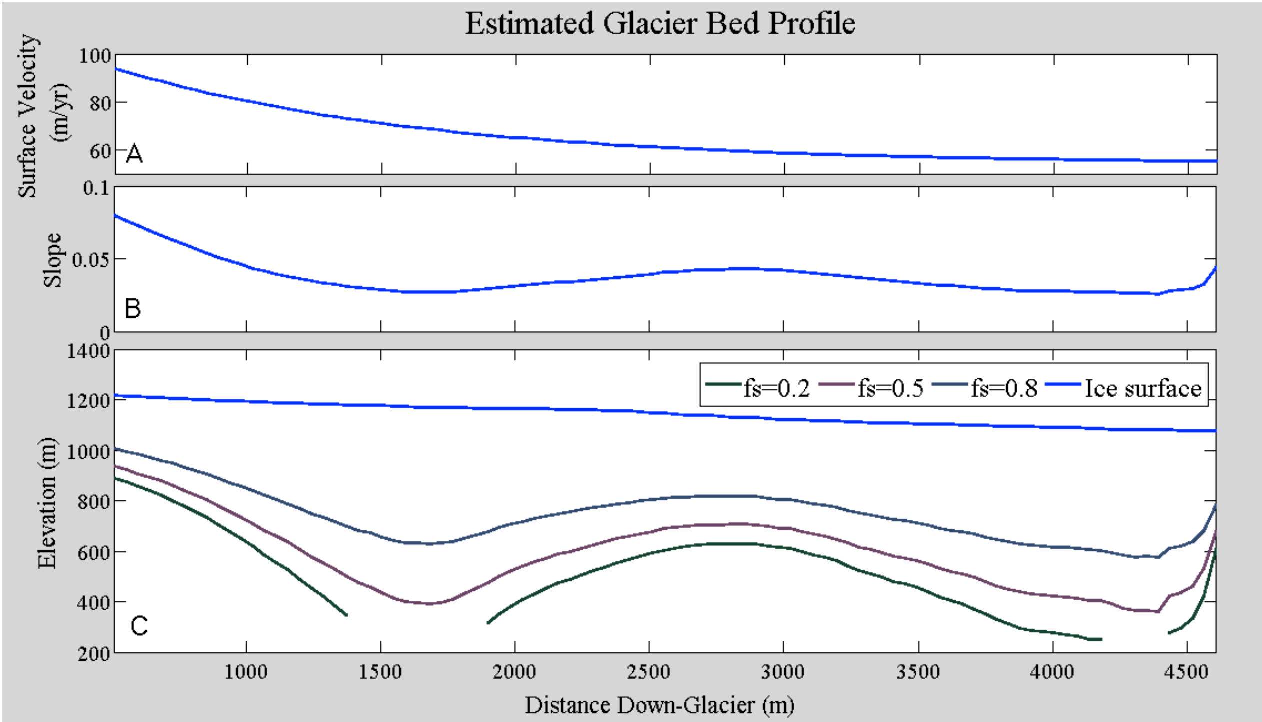

Figure 12. Calculation of bed elevation profile beneath the Gates Glacier centerline. (A) Centerline velocity profile, measured from ogive displacement, and fit to a curve. (B) Smoothed downglacier profile of glacier surface slope from DEM. (C) Elevation profiles of the ice surface and three calculated beds with varying values for the sliding fraction, f_s.

If the sliding component of surface velocity is decreased, the amount of surface velocity due to internal deformation must increase to match the observed surface speed. Given a constant slope, only an increase in ice thickness could accommodate the greater internal deformation. Note that when $f_s = 0.2$, the predicted ice thickness breaches the upper limit of our defined H. As we do not expect a typical glacier to carve a valley that is deeper than its half-width, we can assume that the sliding component of velocity accomplishes more than 20% of total surface velocity. Recent developments in the application of high-powered pixel tracking software to this problem can yield independent, remotely-sensed estimates of glacier sliding velocities (Armstrong et al., unpublished GSA abstract 2013). These external estimates may prove to be essential to future work on this project.

Assuming $f_s = 0.5$, we can now project the initially assumed semi-elliptical shape onto the ice thickness profile to create a 3-D model of the of the Gates Glacier valley (Fig. 13).

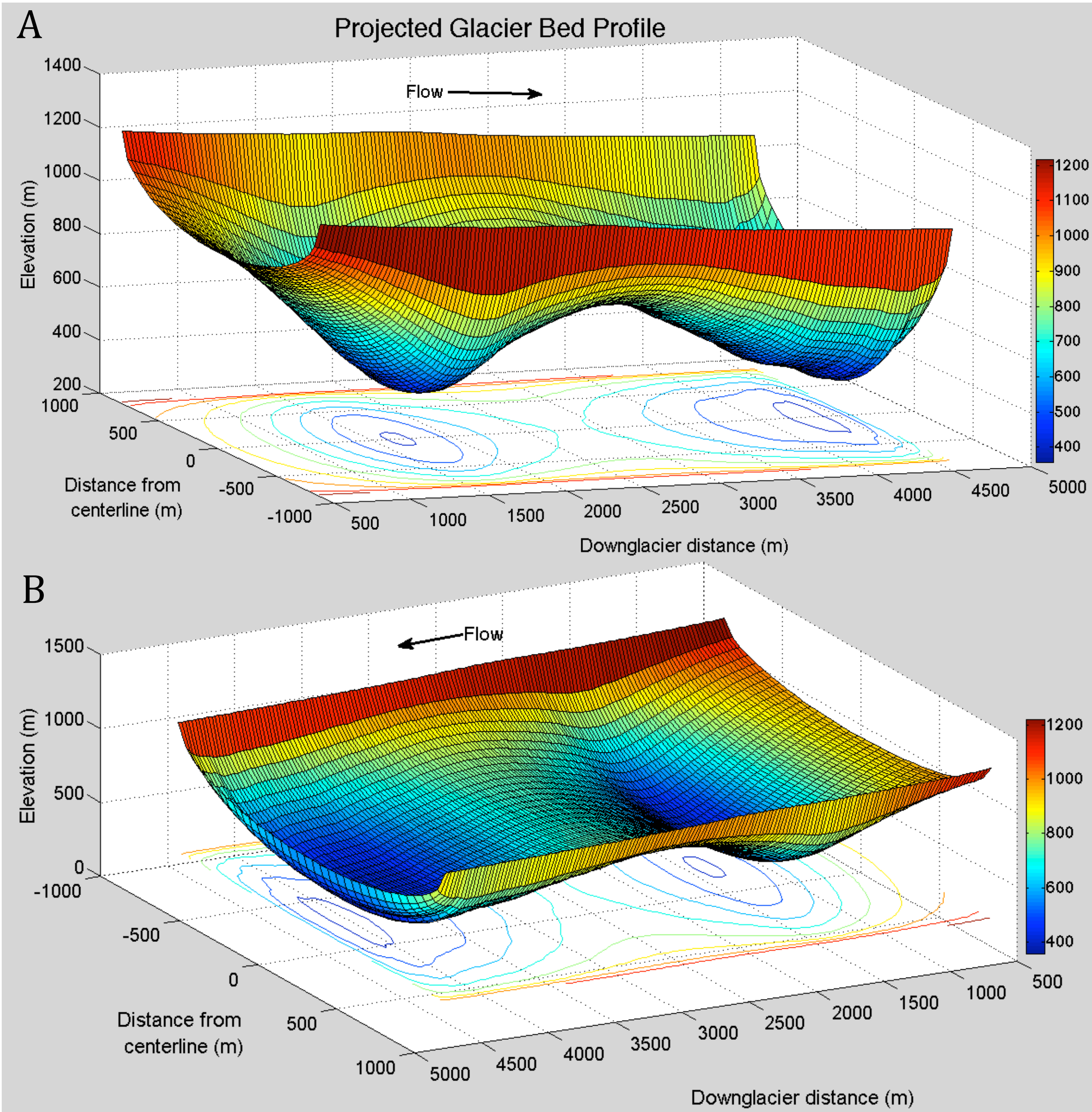

Figure 13. Projected 3-D gates glacier valley profile, viewed from two perspectives. A sliding fraction of $f_s = 0.5$ is assumed. (A) View looking southwest across the calculated Gates valley, emphasizing the magnitude of two over-deepened regions. (B) Oblique view looking northwest across the calculated Gates valley, emphasizing the inner valley geometry.

As expected, the predicted ice thickness increases as the slope decreases. This inverse correlation seems to remain valid, conceptually as well as mathematically. As we observe in icefalls, increased surface slope produces greater internal deformation velocity and ice thinning due to extensional flow. However, the sub-glacial structure beneath regions of shallow surface slope is more difficult to envision, as slope variations on the surface are subtle. One possibility is that the ice retains a relatively constant thickness, and bed-parallel flow reflects minor changes in bed slope and the surface. But this behavior would never occur; gradients in velocity due to the subtle changes in bed slope would inevitably result in local compressional thickening and extensional thinning. The bed over-deepening predicted by the model is another possibility. In this case, regions of gentle slope are a result of ice 'ponding' in deep basins within the valley. In terms of mass balance, this is logical: both regions must pass the same volume of ice in a given period of time for the glacier to flow regularly. A ponded region moves with low velocity, but has a very large cross-sectional area, while a steep region moves swiftly, and has a small cross-sectional area. Therefore, the ice discharge of a steep, shallow region on a glacier should balance the ice discharge of a gentle, deep region.

Unfortunately, we do not yet have field evidence to corroborate the valley shape and ice thickness of the Gates Glacier. But direct measurements of ice thickness on other glaciers do validate the approach. Seismic reflection profiles on the Taku Glacier in southeastern Alaska reveal ice thicknesses up to 1477 m, which dips to over 600 m below sea level (Nolan et al., 1996). The half-width to ice thickness ratio W/H at this point on the Taku Glacier is approximately 1.22 while the predicted W/H on the Gates Glacier is 1.09. This maximum thickness was found below a region of locally gentle surface slope. King et al. (2008) conducted a seismic reflection and GPR survey on midtre Lovenbreen, Svalbard and found a similar over-deepened region where ice surface slope is gentle. An impressive study from Farinotti et al. (2009) combines dense GPR profiles on four separate glaciers in Switzerland with a method of ice thickness estimation that is very similar to the method presented here. Here the input parameters required are the glacier surface topography, the outlined map-view shape, the geometry of the glacier, and estimates of the mass balance profile. A flux calculated from the 'apparent mass balance' (the integral of the mass balance at any point on the glacier, which the glacier must pass to be in steady state), is combined with the expression for ice flux based on Glen's flow law to extract ice thickness. A comparison of direct measurements with calculated ice thicknesses for Rhonegletscher is given in Figure 13A, and an estimate of ice thickness (based on the Rhonegletscher geometry from both 1929 and 2000) of along a downglacier profile is displayed in Figure 13B. The predicted 2000 and 1929 bed geometries are strikingly similar, verifying the technique. Despite the use of different input parameters, Farinotti et al. (2009) establish a robust relationship between surface slope and over-deepened regions for the Rhonegletscher that is similar to what we have predicted for the Gates Glacier.

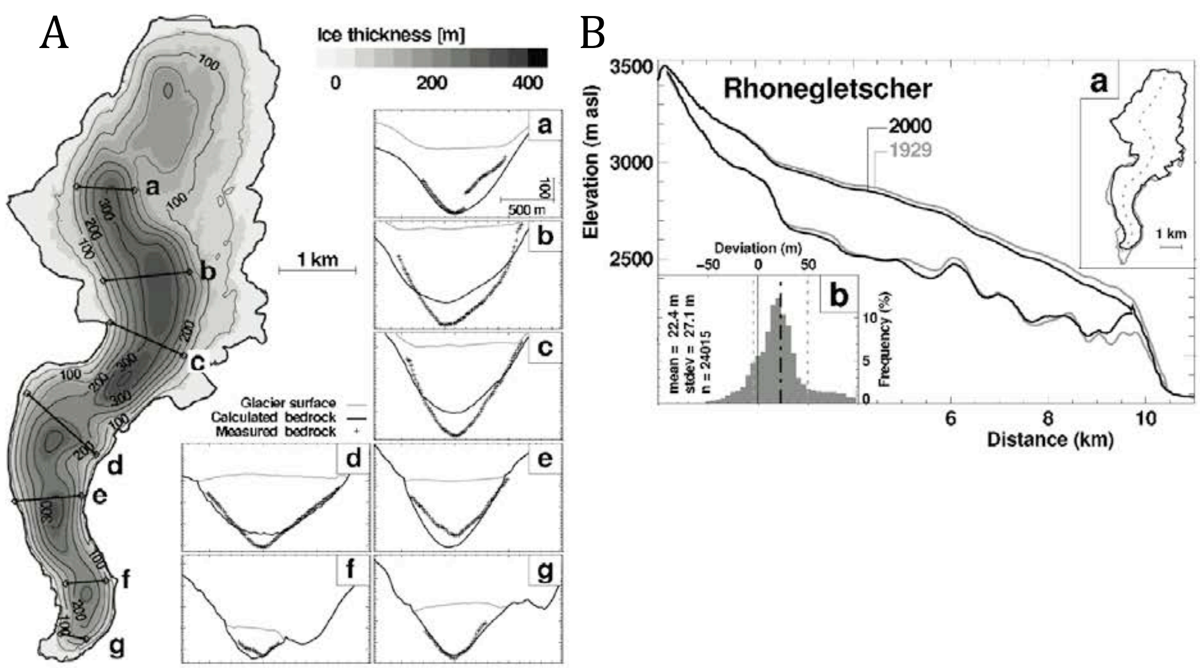

Figure 13. Comparison of similar ice thickness calculation with direct GPR measurements of Rhonegletscher. (A) Locations of seven cross-glacier GPR profiles along Rhonegletscher, with the measured and calculated bed profiles in cross-section. (B) Two calculated downglacier bed elevation profiles based on input geometries from 2000 and 1929. Adapted from Farinotti et al., 2009.

Conclusions

While field campaigns are essential to test hypotheses, they are often expensive and unpredictable. It is therefore expedient for any researcher to obtain as much information that is remotely accessible before embarking on any expedition, as to optimize the efficiency of time spent in the field. This investigation of the Gates Glacier attempts to demonstrate ways in which researchers can explore and further understand glacier behavior with the aid of high-resolution satellite imagery. Primarily, our work establishes ogive analysis as a valuable tool of glaciological study, and has led us to several conclusions:

(i) Ogives are annually forming glacier features that form as ice passes across a significant velocity gradient that is negative to the ice flow direction.

(ii) ArcGIS software, when applied to high-resolution imagery, is adequate to differentiate individual ogives from one another with ease. Some calibration of the Python script is necessary when moving from one glacier image to the next, and the chaotic nature of a glacier surface can result in ogive wavelength errors that have to be corrected by hand.

(iii) Like tree rings, ogives record information about the climatic conditions of the years in which they formed. However, the information embedded within an ogive sequence is still blurred, which suggests it is more complex than a simple dependence on annual weather as captured in time series of temperature or precipitation. We find a rough negative correlation between ogive wavelength and annual temperature, which suggests the interconnectivity of both records to one or more separate, more intricate processes. We propose that the influence of meltwater within the subglacial hydrologic system is a contributing factor to the ogive formation mechanism.

(iv) The mechanism of ogive formation remains unclear, but a possible connection with meltwater induced basal sliding detected within the ogive sequence may lend support to the reverse-faulting mechanism proposed by Goodsell et al. (2002). However, further research on subglacial hydrologic systems and icefall behavior is needed.

(v) The measurement of ogive displacement from repeat imagery yields an easy-to-access downglacier velocity profile. This profile can be applied to calculate longitudinal strain, and even provide an elevation profile of the glacier bed. This bed profile can be modified to yield an estimate of the 3-D geometry of a glacial valley. Continued research on the factors controlling basal sliding velocities are needed for further investigation.

Acknowledgements

Investigation of the Kennicott Glacier is financially supported by a grant from NSF. This project would never have been successful without the close guidance and instruction from R.S. Anderson, the unwavering patience and support of K. Barnhart, and the stimulating conversations with W. Armstrong and L. Anderson.

References

Agassiz, L., On glaciers, and the evidence of their having once existed in Scotland, Ireland, and England, *in* Proceedings Proceedings of the Geological Society of London1840, Volume 3, p. 327-332.

Bartholomaus, T. C., Anderson, R. S., and Anderson, S. P., 2007, Response of glacier basal motion to transient water storage: Nature Geoscience, v. 1, no. 1, p. 33-37.

Bartholomaus, T. C., Anderson, R. S., and Anderson, 2011, Growth and collapse of the distributed subglacial hydrologic system of Kennicott Glacier, Alaska, USA, and its effects on basal motion: Journal of Glaciology, v. 57, no. 206, p. 985-1002.

Bartholomew, I., Nienow, P., Mair, D., Hubbard, A., King, M. A., and Sole, A., 2010, Seasonal evolution of subglacial drainage and acceleration in a Greenland outlet glacier: Nature Geoscience, v. 3, no. 6, p. 408-411.

Clarke, G. K. C., Anslow, F. S., Jarosch, A. H., Radic, V., Menounos, B., Bolch, T., and Berthier, E., 2012, Ice volume and subglacial topography for western Canadian glaciers from mass balance fields, thinning rates, and a bed stress model: Journal of Climate, no. 2012.

Cuffey, K. M., and Paterson, W. S. B., 2010, The physics of glaciers, Access Online via Elsevier.

Farinotti, D., Huss, M., Bauder, A., Funk, M., and Truffer, M., 2009, A method to estimate the ice volume and ice-thickness distribution of alpine glaciers: Journal of Glaciology, v. 55, no. 191, p. 422-430.

Fisher, J. E., 1947, Forbes' and Alaskan" dirt" bands on glaciers and their origin: American Journal of Science, v. 245, no. 3, p. 137-145.

Fisher, J. E., 1962, Ogives of the Forbes type on Alpine glaciers and a study of their origins: Journal of Glaciology, v. 4, p. 53-61.

Forbes, J. D., 1859, Occasional papers on the theory of glaciers.

Godwin, H., Paper read at a Meeting of the Society on 5 February 1949.

Goodsell, B., Hambrey, M. J., and Glasser, N. F., 2002, Formation of band ogives and associated structures at Bas Glacier d'Arolla, Valais, Switzerland: Journal of Glaciology, v. 48, no. 161, p. 287-300.

Harper, J. T., Humphrey, N. F., Pfeffer, W. T., and Lazar, B., 2007, Two modes of accelerated glacier sliding related to water: Geophysical research letters, v. 34, no. 12, p. L12503.

Hubbard, A., Blatter, H., Nienow, P., Mair, D., and Hubbard, B., 1998, Comparison of a three-dimensional model for glacier flow with field data from Haut Glacier d'Arolla, Switzerland: Journal of Glaciology, v. 44, p. 368-378.

Hubbard, A., Bradwell, T., Golledge, N., Hall, A., Patton, H., Sugden, D., Cooper, R., and Stoker, M., 2009, Dynamic cycles, ice streams and their impact on the extent, chronology and deglaciation of the British–Irish ice sheet: Quaternary Science Reviews, v. 28, no. 7, p. 758-776.

King, C. A. M., and Lewis, W. V., 1961, A tentative theory of ogive formation: Journal of Glaciology, v. 3, no. 29, p. 913-939.

King, E. C., Smith, A. M., Murray, T., and Stuart, G. W., 2008, Glacier-bed characteristics of midtre Lovenbreen, Svalbard, from high-resolution seismic and radar surveying: Journal of Glaciology, v. 54, no. 184, p. 145-156.

Leighton, F. B., 1951, Ogives of the East Twin Glacier, Alaska Their Nature and Origin: The Journal of Geology, p. 578-589.

MacGregor, K. R., Anderson, R. S., Anderson, S. P., and Waddington, E. D., 2000, Numerical simulations of glacial-valley longitudinal profile evolution: Geology, v. 28, no. 11, p. 1031-1034.

Miller, M. M., 1949, Progress report of the Juneau Ice Field Research Project, 1948, Dept. of Exploration and Field Research, American Geographical Society.

Nolan, M., and Motkya, R. J., 1995, Ice-thickness measurements of Taku Glacier, Alaska, USA, and their relevance to its recent behavior: Journal of Glaciology, v. 41, no. 139.

Nye, J. F., 1958, A theory of wave formation in glaciers: Physics of the Movement of Ice. IAHS Publications, v. 47, p. 139-154.

Nye, J. F., 1959, The deformation of a glacier below an ice fall: Journal of Glaciology, v. 3, p. 386-408.

Nye, J. F., 1965, The flow of a glacier in a channel of rectangular, elliptic or parabolic cross-section: Journal of Glaciology, v. 5, p. 661-690.

Orowan, E., 1949, Remarks at joint meeting of the British Glaciological Society, the British Rheologists Club and the Institute of Metals: J. Glaciol, v. 1, p. 231-236.

Pfeffer, W. T., Harper, J. T., and O'Neel, S., 2008, Kinematic constraints on glacier contributions to 21st-century sea-level rise: Science, v. 321, no. 5894, p. 1340-1343.
Posamentier, H. W., 1978, Thoughts on ogive formation: Journal of Glaciology, v. 20, no. 82, p. 218-220.
Tyndall, J., 1880, The forms of water, J. Fitzgerald.
Waddington, E. D., 1986, Wave ogives: Journal of Glaciology, v. 32, no. 112, p. 325-334.
Zwally, H. J., Abdalati, W., Herring, T., Larson, K., Saba, J., and Steffen, K., 2002, Surface melt-induced acceleration of Greenland ice-sheet flow: Science, v. 297, no. 5579, p. 218-222.